

This discussion paper is/has been under review for the journal Atmospheric Measurement Techniques (AMT). Please refer to the corresponding final paper in AMT if available.

# Quantification of gas-phase glyoxal and methylglyoxal via the Laser-Induced Phosphorescence of (methyl)GLyOxal Spectrometry (LIPGLOS) method

S. B. Henry<sup>1</sup>, A. Kammrath<sup>1,\*</sup>, and F. N. Keutsch<sup>1</sup>

<sup>1</sup>Department of Chemistry, University of Wisconsin-Madison, 1101 University Avenue, Madison, WI 53706, USA

\*now at: Kimberly-Clark Corporation, 2100 Winchester Road, Neenah, WI 54956, USA

Received: 20 September 2011 – Accepted: 21 September 2011 – Published: 5 October 2011

Correspondence to: F. N. Keutsch (keutsch@chem.wisc.edu)

Published by Copernicus Publications on behalf of the European Geosciences Union.

6159

## Abstract

Glyoxal and methylglyoxal are key products of oxidative photochemistry in the lower troposphere. Reliable measurements of such compounds are critical for testing our understanding of volatile organic compound (VOC) processing in this region. We present  
5 a new method for obtaining sensitive, high time resolution, in situ measurements of these compounds via laser-induced phosphorescent decays. By exploiting the unique phosphorescent lifetimes for each molecule, this method achieves speciation and high-sensitivity quantification of both molecules ( $3\sigma$  limits of detection of 11 ppt<sub>v</sub> in 5 min for glyoxal and 243 ppt<sub>v</sub> in 5 min for methylglyoxal). Additionally, this method enables  
10 the simultaneous measurement of both glyoxal and methylglyoxal using a single, non-wavelength-tunable light source, which will allow for the development of inexpensive and turnkey instrumentation. The simplicity and affordability of this new instrumentation would enable the construction of a long-term, spatially distributed database of these two key species. This chemical map can be used to constrain or drive regional  
15 or global models as well as provide verification of satellite observations.

## 1 Introduction

Glyoxal and methylglyoxal are nearly ubiquitous products of the HO<sub>x</sub>/NO<sub>x</sub> cycle (HO<sub>x</sub> = HO<sub>2</sub> + OH, NO<sub>x</sub> = NO<sub>2</sub> + NO), a photochemically driven oxidation process. This process, which oxidizes volatile organic compounds (VOCs) that are emitted by both  
20 anthropogenic and biogenic sources, has the potential to generate secondary organic aerosol (SOA) precursors and tropospheric ozone (O<sub>3</sub>). Both SOA and O<sub>3</sub> have been shown to have detrimental effects on human health and climate (Lippmann, 1991; Stieb et al., 2000; Lohmann, 2005; Isaksen et al., 2009). In an effort to understand these processes, observations of the VOC oxidation products, as well as the VOCs themselves, provide an important constraint for validating chemical models of the atmosphere by both driving these models as well as being a point of comparison and  
25

6160

identifying inaccuracies within the model mechanism. Glyoxal and methylglyoxal have been shown to partition in appreciable amounts to SOA despite their low molecular weight by reacting to form lower volatility products, such as oligomers or organosulfates, inside the aerosol (Hallquist et al., 2009; Yu et al., 2011). Glyoxal was reported to account for up to 15 % of the mass of SOA in Mexico City (Volkamer et al., 2007).

Glyoxal and methylglyoxal have short lifetimes of a few hours during the day, primarily due to photolysis and reaction with OH (Volkamer et al., 2005a; Fu et al., 2008). Thus, both are tracers of local or regional chemistry since they exist on shorter timescales than large scale transport. They also occur in detectable quantities over much of the planet since they are produced from both anthropogenic and biogenic emissions. The quantities in which they are found are partially due to the fact that they are both products of isoprene, which makes up a large portion (1/3 to 1/2) of globally emitted carbon at an estimated rate of 503 Tg yr<sup>-1</sup> (Guenther et al., 1995). Low tens to low hundreds of ppt<sub>v</sub> for both glyoxal and methylglyoxal have been reported in rural, urban, and marine regions in this work (Sect. 4) and others (Spaulding et al., 2003; Fu et al., 2008; Huisman et al., 2008; Vrekoussis et al., 2009; Sinreich et al., 2010). However, glyoxal concentrations in Mexico City have been recorded as high as low ppb<sub>v</sub> levels (Volkamer et al., 2005a).

Several techniques already exist for detection of these important dicarbonyls. Scanning Imaging Absorption Spectrometer for Atmospheric Cartography (SCIAMACHY), Global Ozone Monitoring Experiment (GOME) and GOME-2 on satellites are used to retrieve global glyoxal datasets (Wittrock et al., 2006; Vrekoussis et al., 2009, 2010); however, validation of these satellites retrievals with ground-based measurement is required for data quality purposes. The Madison Laser-Induced Phosphorescence (Mad-LIP) instrument can acquire high sensitivity (3σ limit of detection (LoD) of 18 ppt<sub>v</sub> per one minute), high time resolution (up to 3 Hz), in situ single point measurements of glyoxal (Huisman et al., 2008). Cavity Enhanced Differential Optical Absorption Spectroscopy (CEDOAS) is also capable of sensitive, fast, in situ single point measurements of both glyoxal (3σ LoD as low as 28.5 ppt<sub>v</sub> per one minute) and methylglyoxal (3σ LoD

6161

as low as 170 ppt<sub>v</sub> per one minute) (Thalman and Volkamer, 2010). A similar spectroscopic method, incoherent broadband cavity enhanced absorption spectroscopy (IB-BCEAS), can achieve a 3σ LoD for glyoxal of 87 ppt<sub>v</sub> in 1 min (Washenfelder et al., 2008). Derivatization using DNPH-coated filters followed by HPLC analysis is a comparatively simple and inexpensive method of detection for both glyoxal (1.5 ppb<sub>v</sub> per four hours) and methylglyoxal (1.3 ppb<sub>v</sub> per four hours), but suffers from high detection limits, poor temporal resolution and potentially significant interferences (U.S. EPA, Center for Environmental Research Information, Research and Development, 1999; Ho and Yu, 2004).

In this study, we present the Laser-Induced Phosphorescence of (methyl)GLyOxal Spectrometry (LIPGLOS) method, a novel, sensitive, and relatively inexpensive method for measuring glyoxal and methylglyoxal that exploits the characteristic distribution of their phosphorescent photons with respect to time. We begin by describing the instrumental setup as well as data collection. We then discuss how the raw data is analyzed to retrieve glyoxal and methylglyoxal signals. The sensitivity is then characterized with a series of calibrations. To validate the concentrations observed by this method, simultaneous glyoxal calibrations of the LIPGLOS method and the Mad-LIP instrument was performed. Finally, an intercomparison of glyoxal data between the two methods during ambient sampling is examined.

## 2 Methods

### 2.1 Measurement principle

The relaxation of a population of excited molecules by any given pathway can be described by:

$$\frac{d[X^*]}{dt} = \frac{-1}{\tau}[X^*] \quad (1)$$

6162

The excited analyte is represented by  $[X^*]$ . The lifetime of the excited state,  $\tau$ , is unique to a specific species undergoing a particular relaxation pathway under a given set of conditions such as temperature, pressure, and in the case of luminescence, quantity of quenching molecules present. The solution to Eq. 1 is an exponential decay, with a decay constant of  $1/\tau$  and a prefactor of  $[X^*]_0$  (initial value of  $[X^*]$ ). During relaxation by luminescence, the intensity of the light emitted is directly proportional to  $[X^*]$ . Therefore, when a population of phosphorescing molecules is observed, the light will have the same temporal distribution as the excited state population; in this case, an exponential decay. If there are more than one phosphorescing species present, each with their own unique lifetime, the temporal distribution of photons is simply the sum of their exponential decays.

The fundamental difference between the LIPGLOS and Mad-LIP methods is how the photon-counting signal is used to derive concentrations. In the latter technique, signals are determined by integrating the phosphorescence signal over the entire decay interval (typically on the order of 10s of  $\mu$ s). As described in more detail below, differentiation of glyoxal and background signals via this technique requires dithering the wavelength of a tunable laser. In contrast, LIPGLOS utilizes the time-dependent decay of the phosphorescence signal to distinguish between these two molecules, allowing for speciation of both compounds at a single wavelength.

## 2.2 Experimental setup

The experimental setup was similar to that of the Mad-LIP instrument, which is described in detail elsewhere (Huisman et al., 2008). The primary differences were the light source as well as additional data collection protocols and hardware as detailed below. Included here is a brief description of the setup, which consists of the main components: light source, detection cell, data acquisition card, and cavity ringdown cell.

6163

### 2.2.1 Light source

Two different light sources were utilized. The first source was a CW, fixed-wavelength diode laser (DL445-050-O, CrystaLaser) which emits 50 mW of 444.457 nm ( $\lambda_{CL}$ ) light with a nominal spectral bandwidth of 1 nm (FWHM) and a TEM<sub>00</sub> beam mode. An optional functionality was added by the manufacturer to allow turning the laser on and off by TTL logic. The laser transition time between the on and off states is <10 ns, effectively instantaneous for its application in these experiments. During operation, this laser was held on for 32  $\mu$ s, and turned off for the same duration which resulted in a repetition rate of 15 625 Hz.

The other light source was a custom tunable Ti:Sapphire laser (TU series, Photonics Industries International, Inc.), which was used to generate 440.104 nm ( $\lambda_{T:S,H}$ ) and 440.136 nm ( $\lambda_{T:S,L}$ ) light. The former was chosen because it is centered on a large, sharp ( $\sim$ .06 nm wide) rovibrational absorption feature of glyoxal, and the latter is a nearby position that is off of the feature with an optical cross-section  $\sim$ 3 times lower. The optical cross-section of methylglyoxal is nearly identical (<0.2% different) at either  $\lambda_{T:S,H}$  and  $\lambda_{T:S,L}$  which is  $\sim$ 10.2 and  $\sim$ 3.5 times smaller than the respective glyoxal optical cross-sections (Meller et al., 1991; Volkamer et al., 2005b). The laser operated at 3 kHz, an average power of 60 mW, and a bandwidth of <0.00078 nm.

### 2.2.2 Detection cell

The excitation light was aligned into a White-type multipass cell which allows for a longer absorption path length, thereby improving instrument sensitivity. The average light power directed into the cell was typically  $\sim$ 40% of power emitted from the laser. For both lasers, this reduction in power was due to scatter/absorption by optics and two beam splitters: one to direct power to the cavity ringdown cell (Sect. 2.2.4) and another to a wavelength meter. An additional power loss unique to the CrystaLaser is incurred since it is operated with a duty cycle of 50%, resulting in a factor of 2 power loss from its CW rated 50 mW. During operation, 32 passes are used through the volume of the cell which ambient air is drawn ( $\sim$ 1/2 L). Phosphorescence photons were

6164













- 715–737, doi:10.5194/acp-5-715-2005, 2005. 6160
- Meller, R., Raber, W., Crowley, J. N., Jenkin, M. E., and Moortgat, G. K.: The UV-visible absorption spectrum of methylglyoxal, *J. Photoch. Photobio. A*, 62, 163–171, 1991. 6164
- O’Keefe, A. and Deacon, D. A. G.: Cavity Ring-down Optical Spectrometer for Absorption-Measurements Using Pulsed Laser Sources, *Rev. Sci. Instrum.*, 59, 2544–2551, 1988. 6166
- 5 Sinreich, R., Coburn, S., Dix, B., and Volkamer, R.: Ship-based detection of glyoxal over the remote tropical Pacific Ocean, *Atmos. Chem. Phys.*, 10, 11359–11371, doi:10.5194/acp-10-11359-2010, 2010. 6161
- Spaulding, R. S., Schade, G. W., Goldstein, A. H., and Charles, M. J.: Characterization of secondary atmospheric photooxidation products: Evidence for biogenic and anthropogenic sources, *J. Geophys. Res.-Atmos.*, 108, D4247, 2003. 6161
- 10 Stieb, D. M., Beveridge, R. C., Brook, J. R., Smith-Doiron, M., Burnett, R. T., Dales, R. E., Beaulieu, S., Judek, S., and Mamedov, A.: Air pollution, aeroallergens and cardiorespiratory emergency department visits in Saint John, Canada, *J. Expo. Anal. Env. Epid.*, 10, 461–477, 2000. 6160
- 15 Thalman, R. and Volkamer, R.: Inherent calibration of a blue LED-CE-DOAS instrument to measure iodine oxide, glyoxal, methyl glyoxal, nitrogen dioxide, water vapour and aerosol extinction in open cavity mode, *Atmos. Meas. Tech.*, 3, 1797–1814, doi:10.5194/amt-3-1797-2010, 2010. 6162
- 20 Turro, N. J. and Engel, R.: Quenching of Biacetyl Fluorescence and Phosphorescence, *J. Am. Chem. Soc.*, 91, 7113–7121, 1969. 6170
- U.S. EPA, Center for Environmental Research Information, Research and Development: Compendium of Methods for the Determination of Toxic Organic Compounds in Ambient Air, TO-11A, Center for Environmental Research Information, National Risk Management Laboratory, Office of Research and Development, U.S. EPA, Cincinnati, OH, 2 Edn., 1999. 6162
- 25 Volkamer, R., Molina, L. T., Molina, M. J., Shirley, T., and Brune, W. H.: DOAS measurement of glyoxal as an indicator for fast VOC chemistry in urban air, *Geophys. Res. Lett.*, 32, L08806, 2005a. 6161
- Volkamer, R., Spietz, P., Burrows, J., and Platt, U.: High-resolution absorption cross-section of glyoxal in the UV-vis and IR spectral ranges, *J. Photoch. Photobio. A*, 172, 35–46, 2005b. 6164
- 30 Volkamer, R., San Martini, F., Molina, L. T., Salcedo, D., Jimenez, J., and Molina, M. J.: A missing sink for gas-phase glyoxal in Mexico City: Formation of secondary organic aerosol,

6175

- Geophys. Res. Lett.*, 34, doi:10.1029/2007GL030752, 2007. 6161
- Vrekoussis, M., Wittrock, F., Richter, A., and Burrows, J. P.: Temporal and spatial variability of glyoxal as observed from space, *Atmos. Chem. Phys.*, 9, 4485–4504, 2009, <http://www.atmos-chem-phys.net/9/4485/2009/>. 6161
- 5 Vrekoussis, M., Wittrock, F., Richter, A., and Burrows, J. P.: GOME-2 observations of oxygenated VOCs: what can we learn from the ratio glyoxal to formaldehyde on a global scale?, *Atmos. Chem. Phys.*, 10, 10145–10160, doi:10.5194/acp-10-10145-2010, 2010. 6161
- Washenfelder, R. A., Langford, A. O., Fuchs, H., and Brown, S. S.: Measurement of glyoxal using an incoherent broadband cavity enhanced absorption spectrometer, *Atmos. Chem. Phys.*, 8, 7779–7793, doi:10.5194/acp-8-7779-2008, 2008. 6162
- 10 Wittrock, F., Richter, A., Oetjen, H., Burrows, J., Kanakidou, M., Myriokefalitakis, S., Volkamer, R., Beirle, S., Platt, U., and Wagner, T.: Simultaneous global observations of glyoxal and formaldehyde from space, *Geophys. Res. Lett.*, 33, doi:10.1029/2006GL026310, 2006. 6161
- 15 Yu, G., Bayer, A. R., Galloway, M. M., Korshavn, K. J., Fry, C., and Keutsch, F. N.: Glyoxal and methylglyoxal in aqueous ammonium sulfate solutions: products, kinetics and hydration effects, *Environ. Sci. Technol.*, submitted, 2011. 6161
- Zalicki, P. and Zare, R. N.: Cavity ring-down spectroscopy for quantitative absorption measurements, *J. Chem. Phys.*, 102, 2708–2717, 1994. 6167

6176

**Table 1.** Summary of the results from the six different calibrations with only either glyoxal or methylglyoxal present inside the detection cell. All data presented here is 5 min integration. Data taken at  $\lambda_{CL}$  has been scaled from 15 min integration to 5 min for purpose of comparison. For purposes of comparison, Mad-LIP has an extrapolated  $3\sigma$  LoD of 1 ppt<sub>v</sub> per 5 min.

Species	$\lambda$	$\sigma$ (cm <sup>2</sup> molecule <sup>-1</sup> )	Sensitivity (prefactor ppt <sub>v</sub> <sup>-1</sup> mW <sup>-1</sup> )	Intercept (prefactor ppt <sub>v</sub> <sup>-1</sup> mW <sup>-1</sup> )	$R^2$	$3\sigma$ LoD (ppt <sub>v</sub> )
Glyoxal	T:S,H	$10.20 \times 10^{-19}$	$(1.5_0 \pm 0.1) \times 10^{-2}$	$-0.4_0 \pm 0.3$	0.991	11
	T:S,L	$3.42 \times 10^{-19}$	$(4.0_0 \pm 0.2) \times 10^{-3}$	$-0.4_5 \pm 0.1$	0.996	37
	CL	$1.05 \times 10^{-19}$	$(3.59_8 \pm 0.07) \times 10^{-4}$	$0.04_8 \pm 0.01$	0.999	146
Methyl- glyoxal	T:S,H	$1.00 \times 10^{-19}$	$(6.30_8 \pm 0.07) \times 10^{-4}$	$1.79_4 \pm 0.02$	1.000	322
	T:S,L	$1.00 \times 10^{-19}$	$(6.8_4 \pm 0.3) \times 10^{-4}$	$1.78_8 \pm 0.08$	0.996	269
	CL	$0.96 \times 10^{-19}$	$(1.5_4 \pm 0.1) \times 10^{-4}$	$0.04_2 \pm 0.02$	0.991	243

6177

**Table 2.** Summary of the results from the six different calibrations with both glyoxal and methylglyoxal present inside the detection cell. The last column represents the relative percent difference in sensitivities as determined in a pure calibration versus in a mixture ( $100 \times (\text{Sensitivity}_{\text{mixed}} - \text{Sensitivity}_{\text{pure}}) / \text{Sensitivity}_{\text{pure}}$ ).

Species	$\lambda$	Sensitivity (prefactor ppt <sub>v</sub> <sup>-1</sup> mW <sup>-1</sup> )	Intercept (prefactor ppt <sub>v</sub> <sup>-1</sup> mW <sup>-1</sup> )	$R^2$	Sensitivity Difference (%)
Glyoxal	T:S,H	$(1.27_3 \pm 0.07) \times 10^{-2}$	$-0.1_8 \pm 0.2$	0.977	-15.1
	T:S,L	$(3.7_9 \pm 0.1) \times 10^{-3}$	$-0.43_5 \pm 0.07$	0.989	-5.3
	CL	$(2.8_9 \pm 0.4) \times 10^{-4}$	$-0.05_8 \pm 0.09$	0.905	-19.7
Methyl- glyoxal	T:S,H	$(2.5 \pm 3) \times 10^{-4}$	$0.4_2 \pm 0.4$	0.064	-60.3
	T:S,L	$(5.2 \pm 1) \times 10^{-4}$	$1.2_8 \pm 0.2$	0.539	-24.0
	CL	$(1.5_2 \pm 0.2) \times 10^{-4}$	$0.07_2 \pm 0.06$	0.944	-1.3

6178

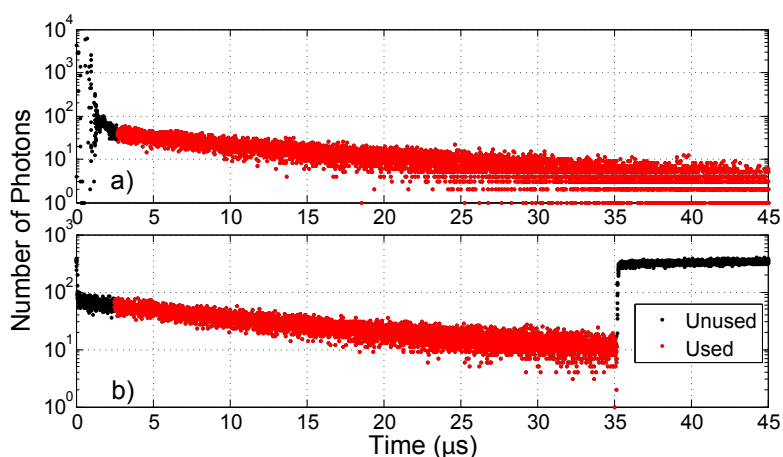


**Fig. 1.** (a) Example histogram corresponding to 1000 ppt<sub>v</sub> glyoxal collected with Ti:Sapphire laser in 5 min. The initial large peak is the laser pulse. (b) Example histogram corresponding to 4200 ppt<sub>v</sub> glyoxal collected with Crystalaser in 15 min. Both the initial peak as well as the plateau after the used data results from laser scatter.

6179

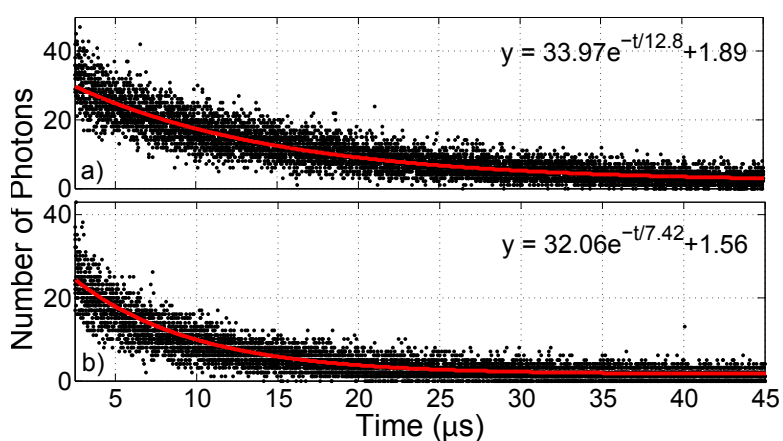


**Fig. 2.** Examples of decays for 5 min integration for glyoxal ((a), 290 ppt<sub>v</sub>) and methylglyoxal ((b), 5400 ppt<sub>v</sub>) taken with the Ti:Sapphire laser with lines of best fit to Eq. (3).

6180

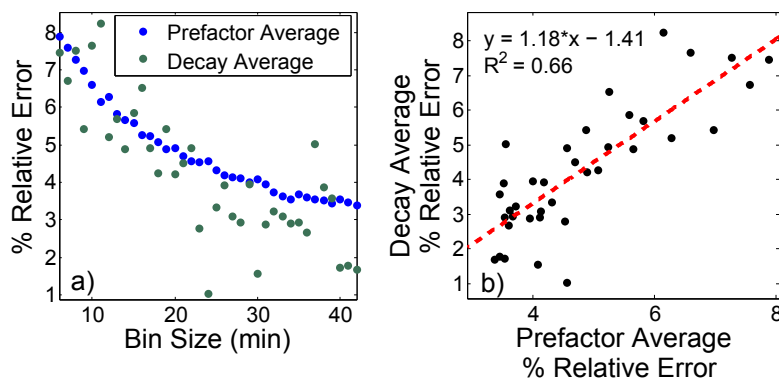


**Fig. 3.** Comparison between the two methods of averaging: prefactor averaging, where the decays of shortest integration are fit followed by averaging the prefactors to desired time resolution, and decay averaging, where the decay is averaged over desired period of integration followed by fitting. **(a)** The percent relative errors for the two averaging methods versus the averaging bin size. **(b)** The correlation between the relative errors in the two averaging methods with the accompanying trend line and equation.

6181

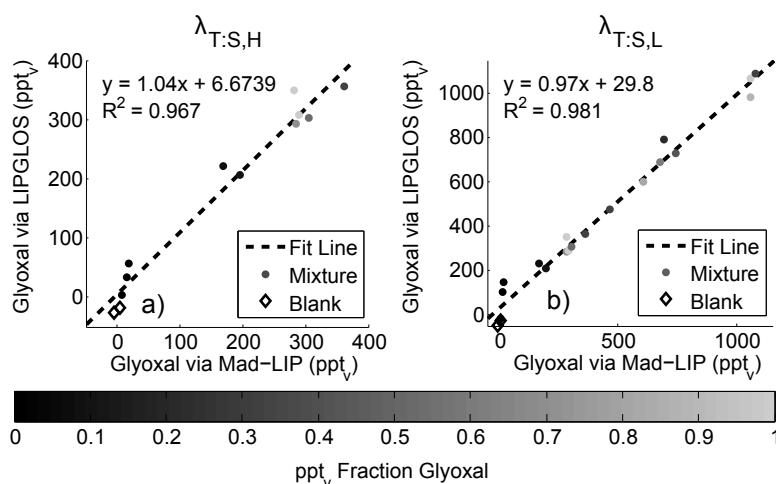


**Fig. 4.** **(a)** Mixing ratio determined by lifetime method at  $\lambda_{T:S,H}$  versus the Mad-LIP determined concentrations during a simultaneous calibration. **(b)** Analogous graph for  $\lambda_{T:S,L}$ . The color bar represents the fraction of total glyoxal and methylglyoxal ppt<sub>v</sub> is glyoxal.

6182

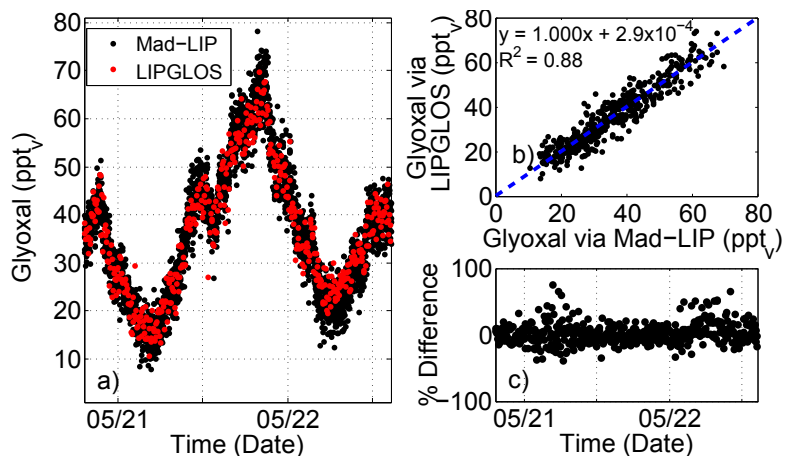


**Fig. 5.** (a) Glyoxal concentration time series from both Mad-LIP (40 s integration) and LIPGLOS (80 s integration). During early morning of the 21st when the concentrations are at their lowest, the standard deviation of the LIPGLOS and Mad-LIP data is 4.2 ppt<sub>v</sub> (extrapolated) and 2.9 ppt<sub>v</sub> in 40 s, respectively. (b) Correlation of measurements coincident within 5 min. (c) Difference between LIPGLOS and Mad-LIP normalized to Mad-LIP measured glyoxal. During the day time hours, the standard deviation of the difference is 8%. During the night, the deviation increases when the noise of the measurement allows values close to zero in the normalization value (glyoxal determined by Mad-LIP).